Int J Adv Manuf Technol (2015) 80:1127–1135
DOI 10.1007/s00170-015-7113-3

ORIGINAL ARTICLE

Chip formation mechanism and machinability of wrought duplex stainless steel alloys

J. Nomani[1] · A. Pramanik[2] · T. Hilditch[1] · G. Littlefair[1]

Received: 21 December 2012 / Accepted: 1 April 2015 / Published online: 15 April 2015

Abstract This paper investigates the chip formation mechanism and machinability of two-phase materials, such as, wrought duplex stainless steel alloys SAF 2205 and SAF 2507. SEM and optical microscopic details of the frozen cutting zone and chips revealed that the harder austenite phase dissipates in the advancement of the cutting tool, being effectively squeezed out of the softer ferrite phase. Microhardness profiles reveal correlation in hardness from the workpiece material transitioning to the chip. The tool wear (TiAlN+TiN coated solid carbide twist drill) and machining forces were investigated. Tool wear, was dominantly due to the adhesion process which developed from built-up edge formation, is highly detrimental to the flank face. Flute damage was also observed as a major issue in the drilling of duplex alloys leading to premature tool failure. Duplex 2507 shows higher sensitivity to cutting speed during machining and strain hardening at higher velocity and less machinability due to presence of higher percentage of Ni, Mo and Cr.

Keywords Duplex stainless steel · Chip formation mechanism · Machinability

1 Introduction

Duplex stainless steel alloys are a result of the continuous attempts to develop new engineering materials with improved properties. In the family of stainless steels, duplex exists between austenite and ferrite stainless steels. Duplex stainless steels are known to have a good resistance to localised corrosion, especially for the high level of chromium (and for some of them molybdenum) and low level of sulphur. The low level of sulphur provides good toughness and a good hot workability for these grades [1]. Duplex stainless steel combines the inherent benefits of both α-ferrite and γ-austenite phases. The α-ferrite phase contains a body-centred cubic crystal structure. This phase in duplex is responsible for the excellent pitting and crevice corrosion resistance properties. While the γ-austenite phase, a face-centred cubic microstructure promotes the superior strength and toughness [2]. Duplex stainless steels generally consist of equal amounts of α-ferrite and γ-austenite phases as shown in Fig. 1. The demand for duplex stainless steels is ever increasing with wide ranging applications due to the materials unique two-phase microstructure. Duplex grades are also less expensive than the more popular austenitic grades, requiring lower amounts of alloying nickel content. Recent development reported in the construction sector indicates emerging applications of duplex stainless steels in structural design [3]. The existence of unresolved issues in machining these alloys becomes apparent, considering its relatively more recent introduction. It is apparent that further applications of duplex stainless steels will require continual development in machining technology [4]. There are only very limited research available on machining of these alloys.

Bordinassi et al. [5] studied the effects of the turning in the superficial integrity of the duplex stainless steel ASTM A890-6A. No microstructural changes in the material were noted due to machining process even when the larger cutting parameters were used. The smaller feed rate (0.1 mm/rev), cutting speed (110 m/min) and cutting depth (0.5 mm) provided smaller tensile residual stress, reduced surface roughness and higher microhardness. Jiang et al. [6] measured the grinding

✉ A. Pramanik
alokesh.pramanik@curtin.edu.au

[1] School of Engineering, Deakin University, Waurn Ponds, Australia

[2] Department of Mechanical Engineering, Curtin University, Bentley, WA 6102, Australia

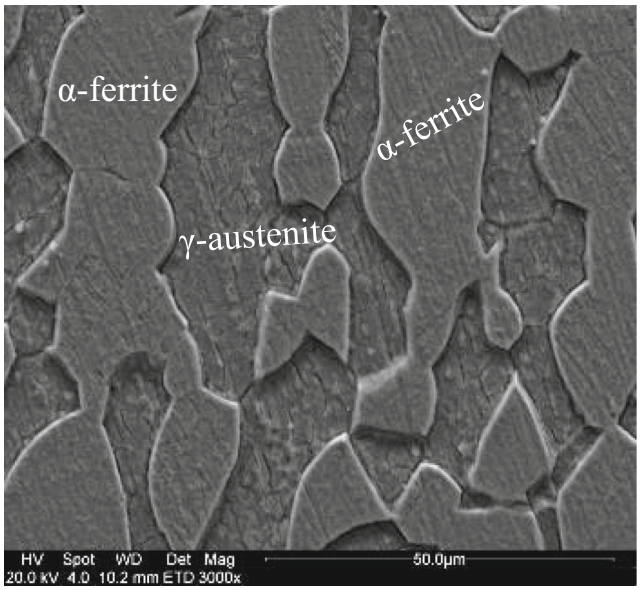

Fig. 1 SAF 2205 duplex microstructure consisting of α-ferrite, γ-austenite phase

ratios, grinding forces and surface roughness of HIPed austenitic (PM 316 L), duplex (PM 2205) and super duplex (PM 2507) as well as as-cast (AC 304) stainless steels during grinding using alumina wheels. Grinding ratio was decreased in the order: AC 304, PM 316 L, PM 2205 and PM 2507 steel, the grinding force increased in the order: AC 304, PM 2205, PM 316 L and PM 2507 steel, the roughness, microcracks and microvoids in the ground surfaces increased in the order: PM 316 L, PM 2205, PM 2507 and AC 304 steel, the ground surface work-hardened increased in the order: AC 304, PM 316 L, PM 2205 and PM 2507 steel. Abrasive particles were found to transfer from the grinding wheel to the ground surfaces. Paro et al. [7] investigated wear and failure mechanisms of TiN-coated cemented carbide tools during drilling of HIPed P/M Duplok 27 and conventionally produced duplex stainless steel ASTM A8190 1A. The machinability of Duplok 27 and A890 1A stainless steels is affected by the formation of built-up edge (BUE), and this causes adhesion wear which is the dominant failure mechanism. The tendency of BUE formation in A890 1A is higher than that of Duplok 27 steel. The life of solid carbide drill with internal coolant supply is between 5 and 12 min and 7 to 20 min for Duplok 27 and A890 1A stainless steel, respectively. Pellegrini et al. [8] reported similar BUE issues with drilling SAF 2205 and made comment on tool manufacturers; they can only stipulate the machining conditions where BUE can be mostly avoided. Nomani et al. [9] investigated drilling of duplex alloys SAF 2205 and SAF 2507, while employing austenite stainless steel 316 L as a benchmark during drilling. It was found that both duplex alloys displayed poorer machinability responses, with 2507 being worst. Abrasion and adhesion are the most common wears appeared on the flank and rake faces. Adhesion wear being the most severe on the flank face was seen to be triggered by built-up edge formation. Duplex alloys 2507 and 2205 both show a higher response to built-up edge formation. Flute damage was found on the drill tool, while drilling both duplex alloys. Higher cutting force and poorer surface finish were found for second generation duplex (2507). Saï et al. [10] analysed the influence of machined surface characteristics of duplex stainless steel on localised corrosion in synthetic sea water. Mechanical surfaces are finished by turning, grinding or burnishing after turning or after grinding. Pitting potential was found to increase for grinded and burnished samples. Residual stresses were tensile in turning and grinding because of the elevation of temperature during machining. Grinding improves surface roughness. Burnishing improved corrosion resistance by giving excellent surface roughness and compressive residual stresses. Potentiostatic polarisation test, a critical pitting temperature test, a SEM-EDS analysis of inclusions and a tool life test were conducted by Jeon et al. [11] to explain the effects of sulphur addition on pitting corrosion and machinability behaviour of super duplex stainless steel containing rare earth metals. The resistance to pitting corrosion decreases with the increase of sulphur content. This is due to the formation of numerous manganese sulphides which deteriorate the corrosion resistance. However, the tool life increases with the increase of sulphur content as the lubricating films of manganese sulphides adheres to tool surface. Renaudot et al. [1] investigated fabrication of long products like bars made of duplex stainless steels. They analysed the effect of sulphur contents as it improves the machinability of stainless steels by forming manganese sulphides in the stainless steels which induce better chip breaking and lubrication at the chip-cutting tool interface. But increase of sulphur content deteriorates the corrosion resistance. Carlborg et al. [12] considered four duplex and one high alloyed austenitic steels during a turning process to compare the performance of cemented carbide cutting tools. Their investigation was limited to qualitative discussion on tool wear and quantitative discussion on tool life. There was no information on machining forces or surface integrity.

Table 1 Nominal chemical composition and mechanical properties of test workpiece alloys (wt%)

Alloy	C	Mn	Si	S	P	Ni	Cr	Mo	Fe	TS (MPa)	HV_{100g}
SAF 2507	0.02	0.74	0.23	0.01	0.02	6.77	25.1	3.68	Balance	866	285
SAF 2205	0.02	0.8	0.4	0.01	0.02	5.2	22.4	3.05	Balance	777	279

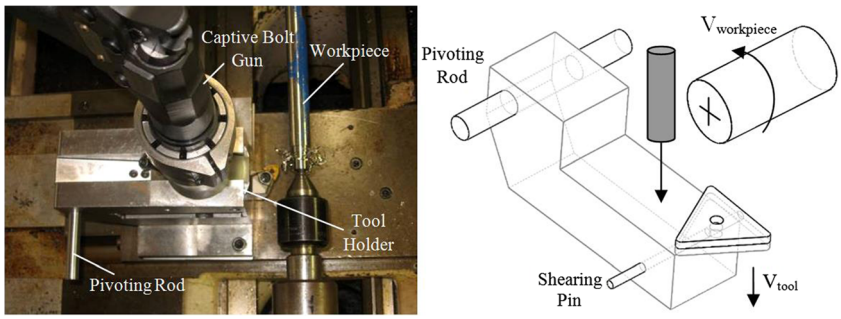

Fig. 2 **a** Experimental setup of quick-stop experiment. **b** Schematic diagram of tool holder and workpiece setup

From the above discussion, it is very clear that there are some investigations on the machining of duplex stainless steels but there is no attempt to investigate the machining mechanism of this material though it is imperatively needed to achieve better understanding and wider application of this potential material. In addition, a systematic analysis of machinability of this material is still missing. There are two long-established issues when machining duplex, the first is its high tendency to form built-up edge, and the second is its high rate of work-hardening. Both issues are highly problematic, leading to undesirables, such as, accelerated tool wear, poor surface finish and unfavourable tolerance levels. In general, machining mechanism and tool wear data are central to the development of cutting technology and cutting-based theoretical models. Hence, the aims of this present study are to (1) analyse the chip formation mechanism of SAF 2205 and SAF 2507 duplex stainless steel alloys, (2) quantitative analysis of tool wear, force and torque during drilling of these two duplex alloys and (3) understand the effect of material compositions on machinability. Table 1 presents the compositions of these two materials. The chip formation mechanism was studied by using a quick-stop device during turning, and machinability was studied in terms of tool wear and machining forces during drilling process.

2 Experimental procedure

An explosive purpose built quick-stop device was mounted to a CNC turning lathe, shown in Fig. 2, for the test. The device comprised of a tool holder held in the position by a pivoting rod and shearing pin. The impact on the tool holder was provided by a captive bolt stunner gun (Cash Special) which shattered the shearing pin while accelerating the tool away from the workpiece during cutting. The velocity of the tool must be greater than the linear velocity of the workpiece to freeze the cutting action effectively. Previous studies on quick-stop devices indicate that the explosive bolt driven devices have a normal upper limit in freezing cutting chips to a maximum cutting velocity of 305 m/min due to issues in deflection [13]. Two cutting speeds, 94 and 65 m/min, well under the reported normal upper limit, were used in quick-stop experiments. The frozen cutting zones were observed under a scanning electron microscope.

Drilling experiments were performed on a CNC machining centre using 12 mm diameter (TiAlN+TiN coated) solid carbide twist drills with internal coolant supply. A general purpose mineral oil-based cutting fluid emulsion with a dilution concentration of 20:1 was supplied at a flow rate of 9.9 L/min. To maintain identical cutting conditions, new drill tools were used to cut each alloy at speed 60 m/min, feed 0.15 mm/rev, depth of cut 30 mm. Thus, the only

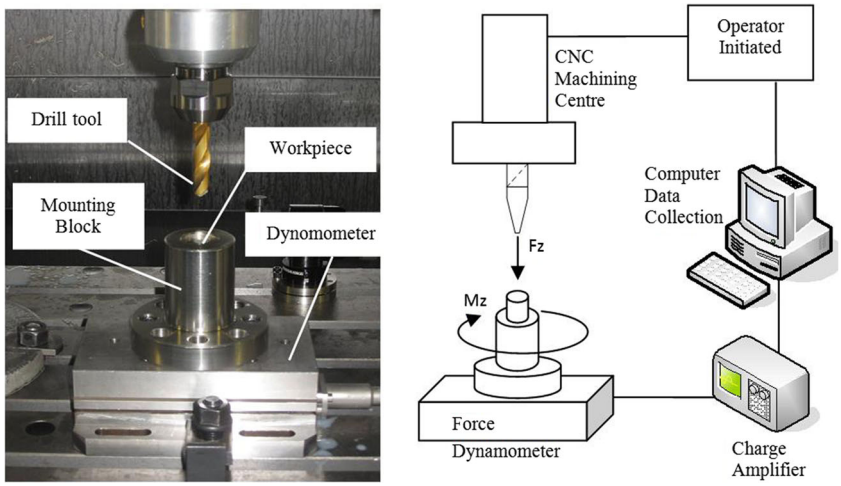

Fig. 3 **a** Drilling experimental setup. **b** Schematic diagram of experimental setup

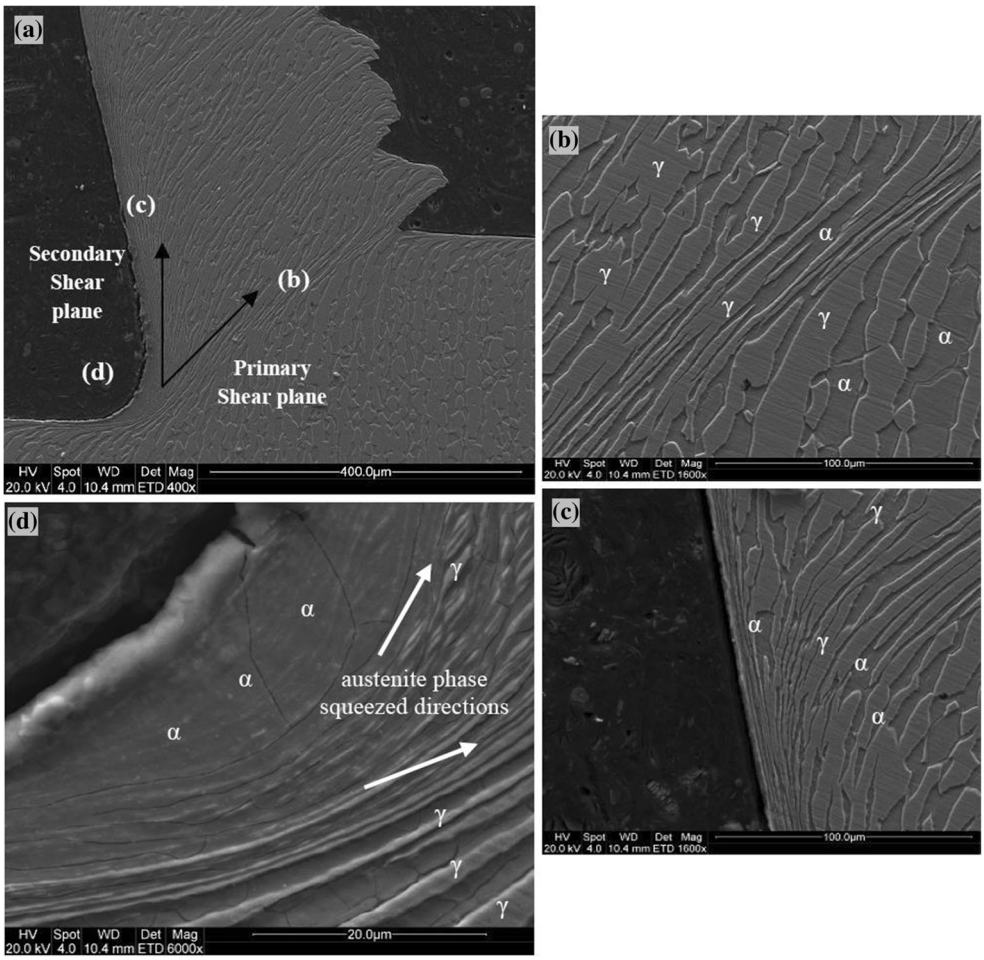

Fig. 4 SEM images of quick-stop specimen SAF 2205 frozen at speed 94 m/min, feed 0.15 mm/rev, undeformed chip thickness 2.5 mm, magnified at various locations α-ferrite, γ-austenite phase. **a** Overview of chip sample at 400× mag; **b** primary shear plane and **c** secondary shear plane at 3000× mag; **d** stagnation zone with built-up edge developing at tip of cutting tool at 6000× mag

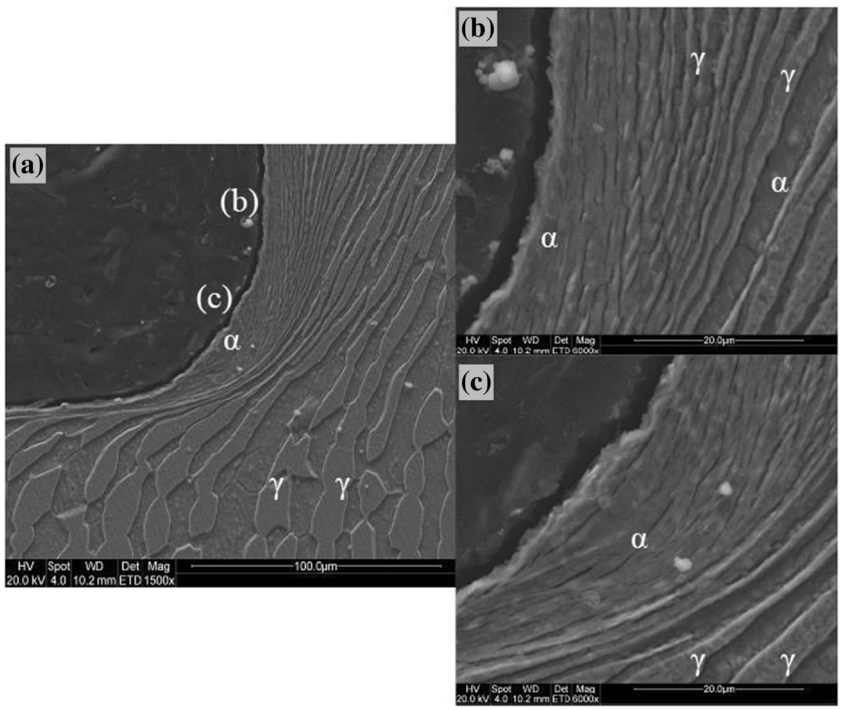

Fig. 5 SEM images of stagnation zone on quick-stop specimen SAF 2507 frozen at speed 94 m/min, feed 0.15 mm/rev, undeformed chip thickness 2 mm, magnified at **a** 1500×, **b** and **c** at 6000×

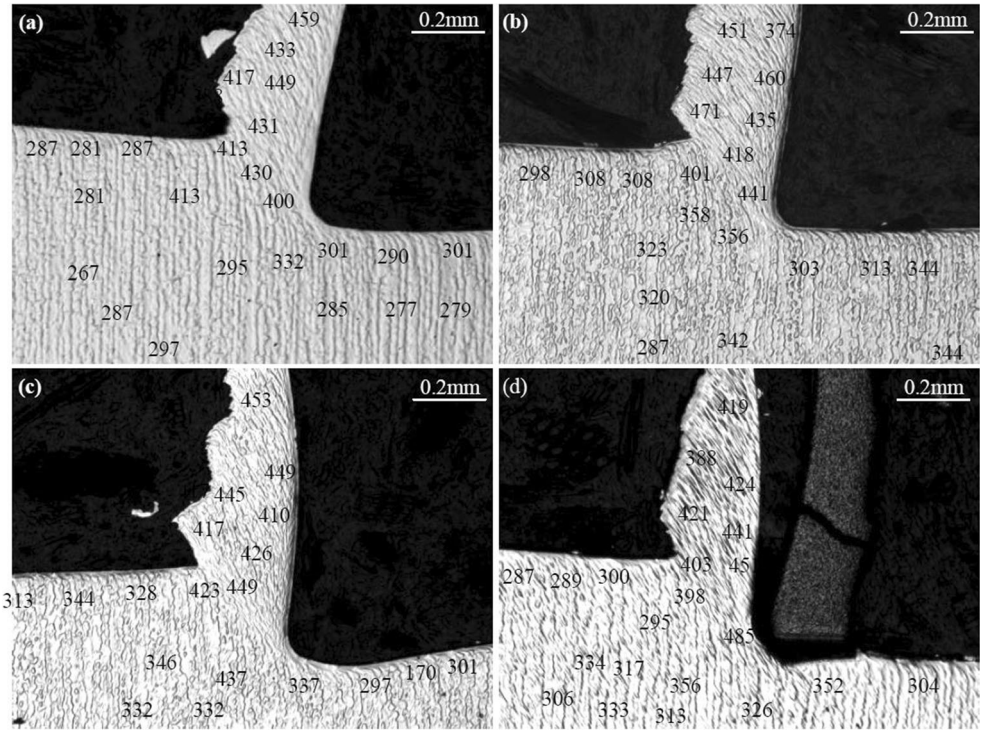

Fig. 6 Knoop microhardness HK300g measurements on quick-stop samples. **a** SAF 2205 and **b** 2507 at speed 94 m/min, **c** SAF 2205 and **d** 2507 at speed 65 m/min

variation in the drilling experiments was the workpiece alloy. Cutting parameters were selected based on the tool manufacturer's recommendations for maximum cutting efficiency for the drill.

Flank wear on both cutting edges of the drill was measured at regular intervals using an optical microscope. Cutting experiments continued until the flank wear reached a set tool wear criterion VB_{max}=0.15 mm or until tool failure. The experimental setup in Fig. 3 shows a cut round-bar workpiece positioned inside a mounting block which is mounted to a force dynamometer (Kistler 9257B) for the measurement of cutting forces. Surface roughness of each machined hole was measured with a stylus surface instrument where the average roughness (Ra) value was recorded.

3 Results and discussion

3.1 Chip formation mechanism

Long continuous serrated chips were produced during turning SAF 2205 at a cutting velocity 94 m/min, feed rate 0.15 mm/rev and undeformed chip thickness 2.5 mm. Figure 4 shows SEM images of a sectioned SAF 2205 quick-stop sampled at a cutting speed 94 m/min. Two shear planes are clearly visible in Fig. 4a. The magnified areas of both the primary and secondary shear planes in Fig. 4b, c show that as the material transitions from the workpiece into the chip, both austenite and ferrite phases undergo rapid deformation and pass into shear

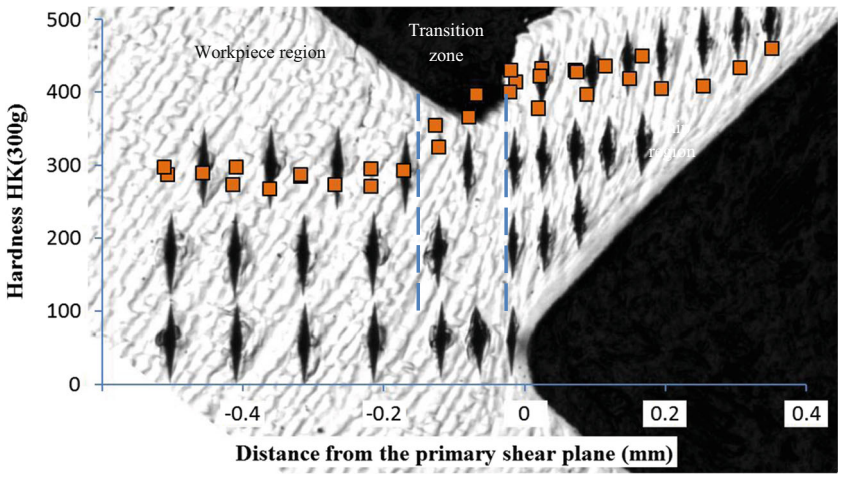

Fig. 7 Correlation of hardness and distance from the primary shear plane for SAF 2205 quick-stop sample frozen at speed 94 m/min

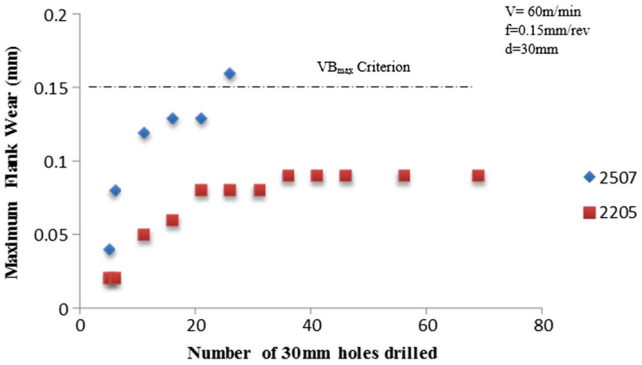

Fig. 8 Maximum flank wear (VBmax) during drilling of SAF 2507 and SAF 2205

zone. Work-hardening is visibly evident in these regions shown by the highly deformed phases at such a very small area. The flow pattern of the material is similar to that of a typical orthogonal cutting. The tip point of the tool region, known as the stagnation zone, is common for material to remain stagnant [14]. This area magnified at 6000× in Fig. 3d shows initial development of built-up edge formation. The clear absence of γ-austenite, the harder phase, is noted in this region. It appears as if the γ-austenite phase is flowing away from the stagnation zone, being effectively squeezed out of the softer α-ferrite phase, into the direction of the shear planes. What remains is built-up edge consisting of α-ferrite and is continually accumulating with the advancement of the cutting tool. This would provide conditions in which there would be a higher chance for built-up edge formation on the tool since the softer phase of the material is more likely to adhere than the harder phase. Naturally, the combination of high forces and elevated cutting temperatures in this region would ultimately lead to the α-ferrite built-up edge forming on the cutting tool over time.

The frozen chip sample of duplex SAF 2507 produced at the identical cutting condition as above is shown in Fig. 5. It appears that the deformation pattern of duplex SAF 2507 during machining is similar to that of duplex SAF 2205. The γ-austenite phase deformed along the shear planes. The absence of austenite is again visible at the stagnation zone region.

3.2 Hardening regions

Knoop microhardness measurements were taken on quick-stop samples after auto polishing to 1 μm. This allowed for grain boundaries to be clearly visible while keeping a contrastingly clear surface for indentation measurements. Readings were taken at various locations on frozen chip samples. Figure 6 shows the measured hardness values of duplex SAF 2205 and 2507 samples, each frozen at two different cutting velocities 94 m/min and 65 m/min, while other cutting parameters remained constant at feed 0.15 mm/rev and undeformed chip thickness 2 mm. As previously mentioned, cutting velocity 94 m/min produced long continuous serrated chips; however, cutting velocity 65 m/min produced helical serrated chips. In general, the profiles in hardness appeared consistent in all samples. The frozen chip sample in Fig. 5d shows remaining fragments of the cutting insert which was fractured during the retraction of the tool. However, the hardness profile generally remains constant. Higher hardness was evident in the chip region compared to that in the workpiece. Maximum hardness measurements were found in SAF 2507 duplex stainless samples. These values were 471 HK at 94 m/min and 485 HK at 65 m/min, compared to 459 HK at 94 m/min and 453 HK at 64 m/min for SAF 2205. The regions of higher and lower hardness are separated by the primary shear plane. Figure 7 describes a general distribution of hardness across the primary shear plane. It illustrates the location of a general transition zone behind the shear plane in the workpiece region. Hardness distribution in this zone indicates that the hardness of workpiece material increases as it moves into the chip region through the primary shear plane. Once the workpiece has passed into the chip region, its hardness has matched that of the chip region. Previous studies have shown this correlation to be common in other metals [15].

If Fig. 6 is analysed carefully, it will be seen that for duplex 2205, the variation of cutting velocity (94–65 m/min) does not influence the hardness notably. On the other hand, if Fig. 6b, d, which present the hardness of duplex SAF 2507 at 94 and 65 m/min, respectively, are compared, it can be observed that the overall hardness of chips at a cutting velocity of 94 m/min

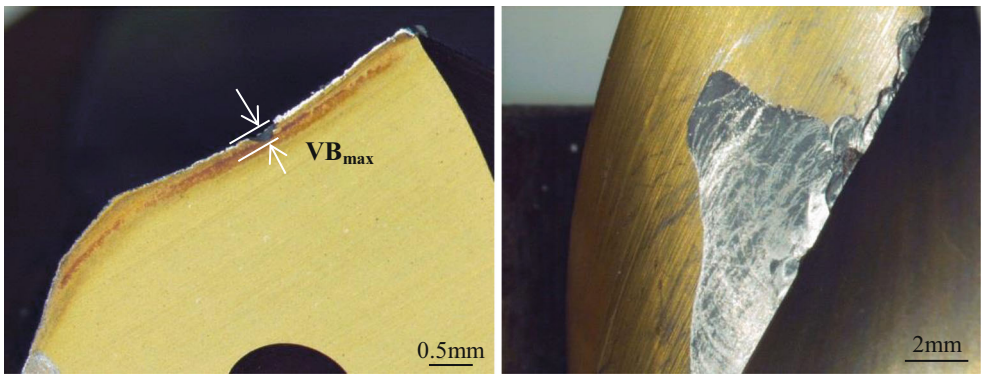

Fig. 9 Optical micrographs of drills used in experimental trials. **a** VBmax criterion reached in cutting SAF 2507 after drilling 26 holes. **b** Flute damage resulting to tool failure in cutting SAF 2205 after drilling 69 holes

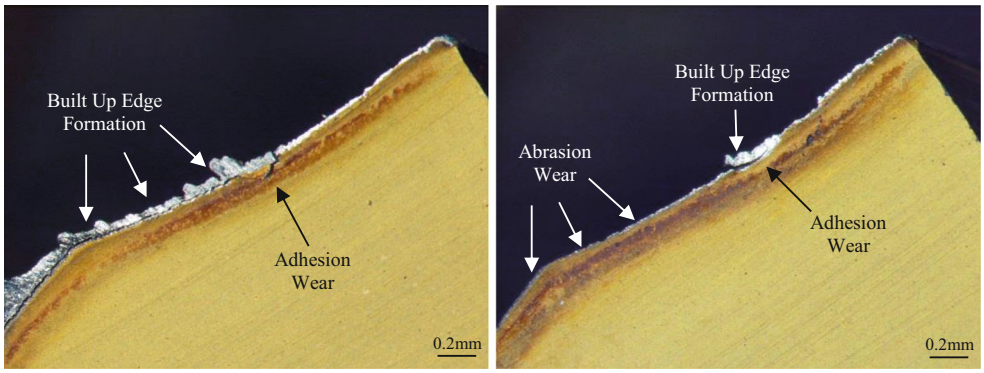

Fig. 10 Built-up edge (BUE) formation on the flank face of a drill tool resulting to adhesion wear in cutting **a** SAF 2507 and **b** SAF 2205

is higher than that of at velocity 65 m/min. This indicates that duplex stainless 2507 has higher sensitivity to velocity during deformation and shows higher strain hardening at higher velocity compare to that of duplex SAF 2205.

3.3 Tool wear

Flank wear results of the drill for both materials are presented in Fig. 8. It indicates that the tool wear and tool wear rate for drilling SAF 2507 are much higher than that of drilling SAF 2205. For SAF 2507, the rate of tool wear is very high at the start of drilling (until 15th hole) then it stabilises (until 23rd hole). The amount of wear (VB_{max}) at this stage is 0.125 mm. After this stabilisation, the wear rate becomes very high and the tool wear reaches the set criterion after a total cutting time of 3.27 min (26 holes) and a measurement of VB_{max} = 0.16 mm, shown in Fig. 9a. Conversely, the initial wear rate of the tool for drilling SAF 2205 was much lower than that of SAF 2507. For this workpiece, the wear rate stabilised after drilling the 20th hole and continued until the 38th hole. The amount of wear at this stage was 0.07 mm which is significantly less at the same point in time than that of SAF 2205. The rate of wear was found to increase again after the 38th hole to 41st hole and then it stabilised again at 0.1 mm until 69th hole. The tool for drilling SAF 2507 showed a cutting time of 8.67 min (69 holes) before the drill succumbed to tool failure. It seems that higher percentage of Ni, Cr and Mo in SAF 2507 contributes significantly higher tool wear compare to that of SAF 2205.

The tool failure for both materials was brought about by significant flute damage located near the tip of the drill, shown in Fig. 9b. The impact of the damage resulted to unpredictable cutting loads and poor chip evacuation during drilling. The flute wear was first evident as a small crater after drilling 16 holes and developed in size over cutting time. Flute wear was also evident on the SAF 2507 drill. However, the relative size and severity was insignificant at the time the drill reached the VB_{max} criterion after 26 holes of drilling.

Tool wear occurring along the flank face was characterised as two main types, adhesion and abrasion wear. Abrasion was the most extensive wear type along the flank face, generated from sliding friction occurring between the drill cutting edge and the chip material flow. Its effect on the cutting edge was observed as minor and at most led to frittering and flaking along the flank and rake face of the tool.

The occurrence of adhesion wear, however, being less frequent as abrasion wear, was more detrimental to the tool cutting edge. It was found major increases in VB_{max} to be primarily caused from adhesion wear development. As shown in Fig. 10, the high tendency for built-up edge (BUE) formation played a significant role in adhesion wear development. Bonding occurred

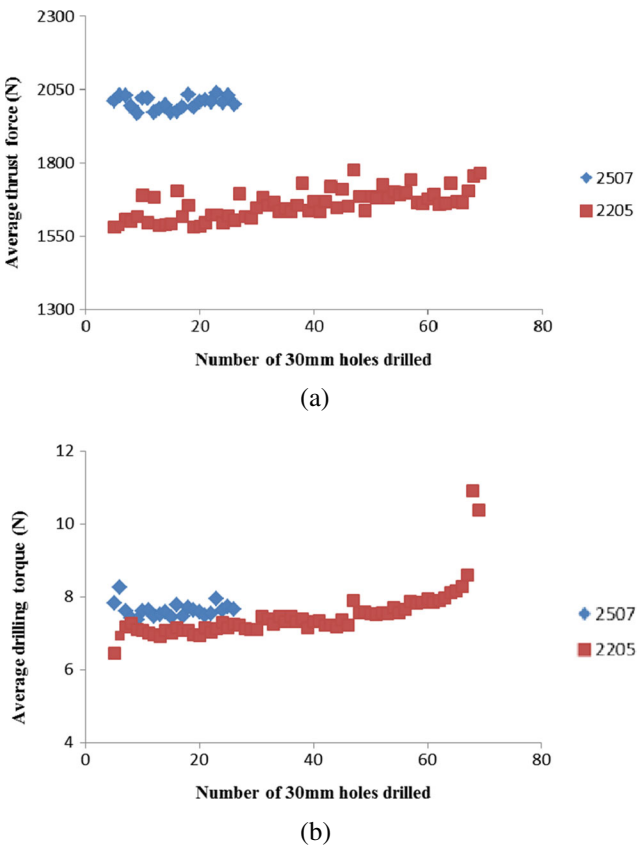

Fig. 11 Comparative average cutting load measurements throughout entire cutting experiments. **a** Thrust force Fz, **b** drilling torque Mz

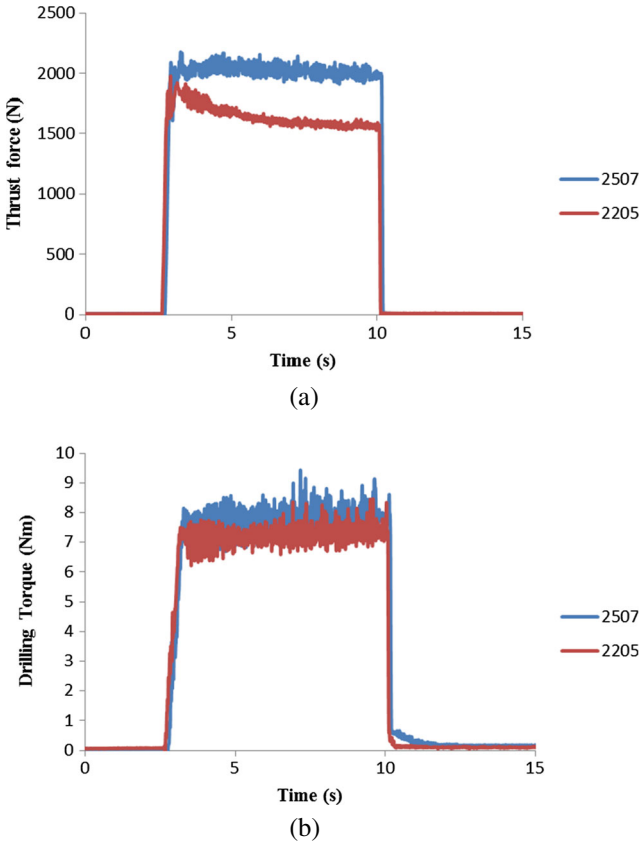

Fig. 12 Comparative measurements taken during a complete drilling of a single hole. **a** Thrust force, **b** drilling torque

between the hardened BUE layer and the drill carbide edge, and it appeared as more cutting occurred, the shearing motion withdrew the BUE layer and 'plucked' off an attached region of the carbide edge leaving behind visible cavities. Duplex SAF 2205 responded with less severity in BUE formation compared to that of duplex SAF 2507 alloy resulting to smaller areas of adhesion wear on its drill tool.

3.4 Machining forces

Average thrust forces are shown in Fig. 11a which appears to indicate and thus confirm that SAF 2507 has a poorer machinability characteristic being the harder material to cut due to higher percentage of Ni, Cr and Mo content. SAF 2205 show an increasing trend in thrust force in the progression of experiments which is accounted by two main influences, effects of tool wear and the altering geometry of the cutting edges due to built-up edge formation. The measured cutting torque provides a general indication of the power consumption since cutting power is the product of the cutting torque and the rotational speed of the drill. Thus, average torque shown in Fig. 11b indicates that more cutting power was required during drilling of SAF 2507 duplex alloys than that of SAF 2205. The significant increase in torque in the final stages of experiments for SAF 2205 demonstrates the severe impact of flute damage which resulted in tool failure as previously discussed. Figure 12 shows typical thrust and torque measurements taken during the complete drilling time of a single hole. The initial accelerated increase in thrust force shown by SAF 2205 reveals poor cutting action of the drill's chisel edge during surface penetration. However, the accelerated thrust force quickly reduced once drilling beyond surface penetration, when the drill's main cutting edges initiate cutting action. SAF 2205 duplex alloy responded better during surface penetration offering less resistance. Drilling torque profile remained consistent in the drilling for each alloy for the entire cutting period. The maximum cutting torque was recorded higher when drilling SAF 2507, as shown in Fig. 12b. The recorded peaks for SAF 2507 was slightly higher than SAF 2205.

4 Conclusion

Conclusions drawn from this investigation are given below.

(a) Built-up edge forming at the stagnation zone consists only of α-ferrite, the softer phase of the material. The harder phase γ-austenite appears to be flowing away from the stagnation zone, while α-ferrite is accumulating with the advancement of the tool tip. Both of the duplex stainless steel alloys show similar chip formation mechanism.
(b) Hardness in both duplex stainless alloys increases from workpiece to the chip region, across the primary shear zone. The size of the transition zone, the region where the hardness increase initiates appears unaffected by cutting speeds ranging between 94 and 65 m/min for duplex SAF 2205. Duplex 2507 shows higher sensitivity to velocity during deformation and strain hardening at higher velocity due to presence of higher percentage of Ni, Mo and Cr.
(c) Adhesion and abrasion wear was the most common wear types appearing on drill flank face during drilling of duplex alloys. Adhesion wear was highly detrimental to the flank face, triggered by the formation of built-up edge appearing on the cutting edge of the drill tool. Duplex 2507 shows higher tool wear due to presence of higher percentage of Ni, Mo and Cr.
(d) Flute damage was observed near the tip of drill tools, in the drilling of both duplex alloys. Tool failure causes unpredictable cutting loads and poor chip evacuation in drilling.
(e) SAF 2205 holds the better machinability in terms of tool wear and cutting power which correlates with mechanical strength and hardness values between these alloys.

References

1. Renaudot N, Chauveau E, Mantel M (2011) Machinability of duplex stainless steels long products: how to deal with the sulphur way? Revue de Metallurgie Cahiers D'Informations Tech 108(4): 245–257
2. Anon, Practical guidelines for the fabrication of duplex stainless steel, International Molybdenum Association (2001)
3. Baddoo NR (2008) Stainless steel in construction: a review of research, applications, challenges and opportunities. J Constr Steel Res 64(11):1199–1206
4. Pramanik A, Islam MN, Basak AK, Littlefair G (2013) Machining and tool wear mechanisms during machining titanium alloys. Adv Mater Res 651:338–343
5. É. C. Bordinassi, M. F.Stipkovic, G. F. Batalha, S.Delijaicov, N. B. D. Lima, Surface integrity analysis in the super duplex stainless steel ASTM-A890 after machining, International Journal of Materials and Product Technology 33(3)(2008)198-212.
6. Jiang L, Paro J, Hänninen H, Kauppinen V, Oraskari R (1996) Comparison of grindability of HIPped austenitic 316 L, duplex 2205 and super duplex 2507 and as-cast 304 stainless steels using alumina wheels. J Mater Process Technol 62(1–3):1–9
7. Paro J, Hänninen H, Kauppinen V (2001) Tool wear and machinability of HIPed P/M and conventional cast duplex stainless steels. Wear 249:279–284
8. Pellegrini G, Caprio G, Pacagnella R (1999) Drilling operations on duplex stainless steels: tool wear analysis. Metallurgia Italiana 91(5):23–30
9. Nomani J, Pramanik A, Hilditch T, Littlefair G (2013) Machinability study of first generation duplex (2205), second generation duplex (2507) and austenite stainless steel during drilling process. Wear 304:20–28
10. W. B. Saï, E. Triki, Influence of machined surface characteristics on a duplex stainless steel corrosion resistance. Transactions of the Canadian Society for Mechanical Engineering 30(2)(2006)183-190.
11. Jeon SH, Kim ST, Lee IS, Park YS (2010) Effects of sulfur addition on pitting corrosion and machinability behavior of super duplex stainless steel containing rare earth metals: part 2. Corros Sci 52(10):3537–47
12. Carlborg C (1991) Machinability of duplex stainless steel. Proc Dup Stainless Steel 1(1):683–96
13. B.J. Griffiths, The development of a quick-stop device for use in metal cutting hole manufacturing processes, International Journal of Machine Tool Design and Research, 26(2)(1986)191-203.
14. Nasr MNA, Ng EG, Elbestawi MA (2007) Modelling the effects of tool-edge radius on residual stresses when orthogonal cutting AISI 316 L. Int J Mach Tools Manuf 47(2):401–411
15. Wright PK, Thangaraj A (1982) Correlation of tool wear mechanisms with new slipline fields for cutting. Wear 75(1):105–122